Evolution of the Laves Phase in Ferritic Heat-Resistant Steels During Long-term Annealing and its Influence on the High-Temperature Strength

NILOFAR NABIRAN, SIMON KLEIN, SEBASTIAN WEBER, and WERNER THEISEN

Heat-resistant ferritic steels containing Laves phase precipitates were designed supported by thermodynamic modeling. High-temperature compression tests at 1173.15 K (900 °C) and a detailed characterization of the microstructural evolution during annealing at 1173.15 K (900 °C) were carried out to investigate the effect of Laves phase formation on the high-temperature strength. Due to the addition of W/Mo and/or Nb, the high-temperature strength of the newly designed alloys is significantly higher than that of the reference steels. However, the high-temperature strength of all investigated steels decreases slightly as the annealing time is increased up to 1440 hours. To determine the influence of Laves phase formation and coarsening on the high-temperature strength during long-term annealing, the precipitates were extracted from the ferritic matrix in different annealing states. The phases in the powder residue were determined by XRD, and the chemical composition of the Laves phase in dependence of the annealing time was analyzed by EDS measurements. During annealing, steel Fe18CrMoW forms Nb(C,N), Ti(C,N), Laves phase (Fe_2Nb) and Fe_3Nb_3C, whereas alloy Fe19CrWAl forms Nb(C,N), Ti(C,N), and Laves phase (Fe_2Nb). The Laves phase within the alloys Fe18CrMoW and Fe19CrWAl differs in its morphology as well as its chemical composition. The Laves phase in steel Fe18CrMoW attains its chemical equilibrium after 192 hours, whereas alloy Fe19CrWAl required 24 hours. Overall, the formation of the Laves phase prevents significant grain growth during high-temperature annealing, thus preserving the high-temperature strength over a long time period.

DOI: 10.1007/s11661-014-2505-9

I. INTRODUCTION

THE application range for high-Cr ferritic steels includes automotive exhaust systems, metallic interconnectors in planar solid oxide fuel cells (SOFC), and heat exchangers in auxiliary power units.[1,2] High-Cr ferritic steels are generally susceptible to intergranular corrosion and embrittlement, which exacerbate steel production and processing.[3,4] Furthermore, ferritic steels exhibit lower high-temperature strength and creep resistance compared to austenitic steels with a similar chromium content. However, due to their lower thermal expansion coefficient, ferritic steels have a higher thermal fatigue resistance compared to austenitic grades.[3,5] Thus, their good corrosion properties and lower costs make the high-Cr ferritic steels suitable for applications with frequent temperature cycling such as automotive exhaust systems. In this case, high-Cr ferritic heat-resistant steels are the most commonly used material and have replaced cast iron, the traditional material for this application.[1,6] This change has been driven by increasing efforts to improve the efficiency of engines and to reduce their weight. Another aim is to reduce air pollution by emitting clean exhaust gas, which involves purging this gas as quickly as possible after starting the engine.[1] Since the efficiency of a catalytic converter is low if its temperature is low, it is important to raise the exhaust gas temperature [$T_{gas} > 1173.15$ K (900 °C)].[1,7] This is why thinner materials are used to reduce the heat capacity of the exhaust system. Due to the lower heat capacity, the exhaust gas flows to the converter with a higher temperature and heats the catalytic converter more rapidly to the active temperature range.[1,8]

However, higher service temperatures and thinner constructions lead to a higher exposure of the material component. Alloy X2CrTiNb18 is currently used for exhaust manifolds, though, its high-temperature strength is not sufficient to allow further reductions in the thickness of the construction element. For this reason, it is important to increase the high-temperature strength of ferritic stainless steels and combine it with their excellent thermal fatigue resistance.

Various strengthening mechanisms can be used to increase the high-temperature strength. One of these is precipitation hardening with formation of a Laves

NILOFAR NABIRAN, Postdoc, SIMON KLEIN, Ph.D. Student, and WERNER THEISEN, Professor, are with the Chair of Materials Technology, Ruhr-University Bochum, Bochum, Germany Contact e-mail: nilofar.nabiran@rub.de SEBASTIAN WEBER, Professor, is with the Chair of New Manufacturing Technologies, Bergische Universität Wuppertal, Solingen, Germany.

Manuscript submitted September 9, 2013.
Article published online October 30, 2014

phase. The concept of Laves phase precipitation to increase the high-temperature strength and creep resistance is known from the 9 to 12 pct Cr ferritic/martensitic heat resistant steels.[9,10] However, the effect of the Laves phase in ferritic stainless steels on the high-temperature strength and creep resistance is discussed in literature controversionally.[1,11,12]

The aim of this work is to increase the high-temperature strength of high-Cr ferritic steel. Three new materials containing the intermetallic Fe_2Nb-type Laves phase were designed and investigated. The present study focuses on the effect of Laves phase formation, coarsening, and chemical evolution in dependence of the annealing time on the high-temperature strength.

II. EXPERIMENTAL

A. *Alloy Modeling and Manufacturing*

The alloys were designed with thermodynamic modeling software Thermo-Calc®, which is based on the CALPHAD method.[13] This software was used for calculating phase equilibria and evaluating phase stabilities to determine the influence of various alloying elements, such as Nb, Si, Mo, and W. All calculations were carried out with the TCFe6.2 database.[14]

The alloys Fe18CrW, Fe18CrMoW, and Fe19CrWAl investigated in the present work are newly designed heat-resistant ferritic steels. Their chemical composition is shown in Table I. Alloys Fe18CrW and Fe18CrMoW were produced by vacuum induction melting with a weight of about 100 kg by Outokumpu Nirosta (formerly ThyssenKrupp Nirosta). The castings were hot-rolled to a thickness of 4 mm. Alloy Fe19CrWAl was also produced by vacuum induction melting with a weight of about 100 by Outokumpu VDM (formerly ThyssenKrupp VDM). It was hot-rolled to a thickness of 17 mm. Consequently, hot-rolled material was used to investigate the high-temperature strength.

B. *Heat Treatment*

To investigate the influence of the formation and coarsening of the Laves phase on the mechanical properties, all specimens were solution-annealed (s-a) at 1373.15 K (1100 °C) for 5 minutes, quenched in water, and then isothermally annealed under ambient atmosphere at 1173.15 K (900 °C) for dwell times ranging from 1 to 1440 h.

C. *Mechanical Tests*

Compression tests were performed to determine the high-temperature strength as a function of aging time. Cylindrical specimens with 4 mm diameter and 10 mm length were used. After isothermal annealing at different dwell times, hot compression tests were carried out at 1173.15 K (900 °C) with a thermomechanical testing device. The specimens were heated to 1173.15 K (900 °C) with a heating rate of 5 K and thermally equilibrated for 2 minutes. Compression was performed with an initial engineering strain rate of 0.001 s^{-1} to a maximum deformation of 10 pct. The specimens were cooled to room temperature with a cooling rate of 15 K after compression.

D. *Microstructural Investigations*

The microstructure in all states was characterised by light optical microscopy and scanning electron microscopy. Scanning electron microscopy was carried out with a Leo-1530 VP SEM equipped with a LaB_6 field emission gun and a Pegasus EDAX system. Secondary electron contrast was used to detect precipitates, and a backscattering detector was used for general microstructural characterisation.

The grain size was measured using the standard linear intercept method at magnifications of 50 and 100 times, as described in DIN EN ISO 643. The average grain

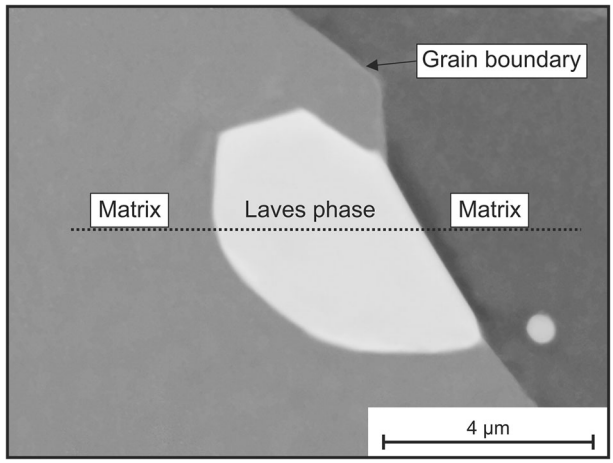

Fig. 1—Laves phase precipitate in steel Fe18CrMoW after annealing for 1440 h at 1173.15 K (900 °C). The dotted line marks the EDS linescan.

Table I. Chemical Composition of the Investigated Alloys (mass percentage)

Alloy	C	N	Cr	Nb	Si	W	Mo	Ti	Al	Hf	Zr	Y	La
Fel9CrWAl	0.013	0.007	18.80	0.69	0.29	2.07	—	0.02	3.20	0.05	0.04	0.05	—
Fel8CrW	0.018	0.020	18.20	0.85	0.62	1.80	—	0.06	—	—	—	—	—
Fel8CrMoW	0.019	0.020	17.90	0.85	0.63	1.40	0.50	0.06	—	—	—	—	—
XlCrWNbTiLa22	0.007	0.015	22.93	0.51	0.21	1.94	—	0.07	—	—	—	—	0.080
X2CrTiNbl8	0.017	0.020	17.84	0.39	0.65	—	—	0.14	—	—	—	—	—

diameter was determined with a minimum of three images and a total number of at least 180 grains per image. Quantitative investigations of precipitates were supported by the software a4i Analysis. The projected area A of the particles and their diameter were determined automatically by means of binary image conversion. Three images from each annealing state with more than 1500 precipitates per image were used for these measurements. The average diameters of the precipitates were determined by measuring the minimum and maximum projected diameters (d_{min}/d_{max}), respectively, of all particles in the images.

E. *Residue Extraction of Precipitates*

For further analysis of their morphology and chemistry, Laves phase precipitates were electrochemically extracted from alloys Fe18CrW, Fe18CrMoW, and Fe19CrWAl. A mixture of 1 vol pct tetramethylammonium chloride and 10 vol pct acetylacetone in methanol was used as the electrolyte.[15,16] After contacting at −1244 μV, the specimens were etched for about 10 hours with a potential of 200 μV versus a calomel electrode and with an auxiliary platinum electrode. In the next step, the precipitates were isolated from the electrolyte using a polyethylene membrane filter with a pore size of 0.2 μm fitted to Büchner funnel and flask. The residue was then dispersed in methanol, pipetted onto a copper carrier, and dried in a vacuum desiccator.

The extracted residue was used to identify the precipitates by means of X-ray diffraction (XRD) with an CuK_α tube (λ = 1.54178 Å). The chemical composition of the precipitate residue (Laves phase) was determined by energy dispersive X-ray spectrometry (EDS) in the SEM and by inductively coupled plasma optical emission spectrometry (ICP-OES).

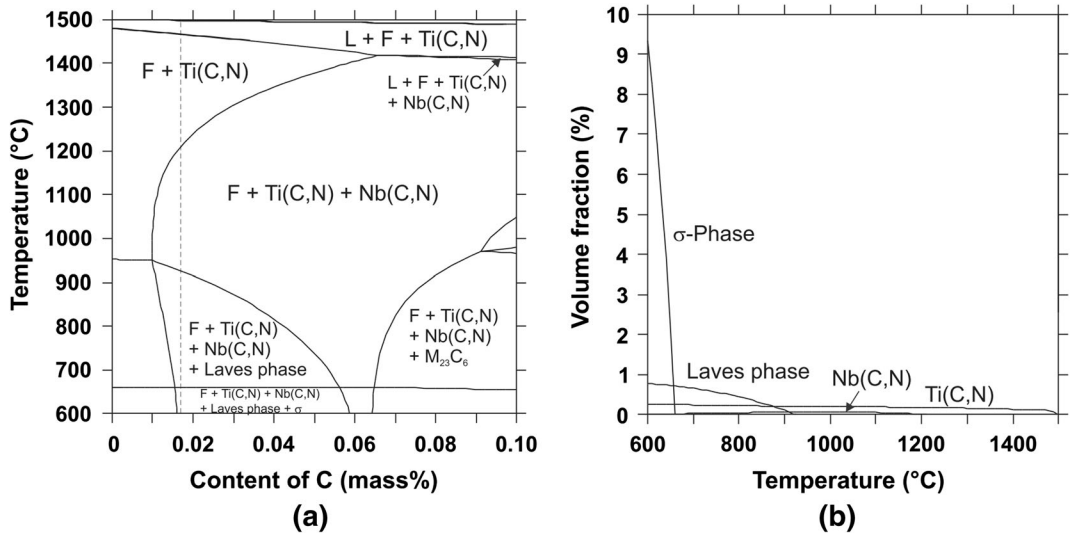

Fig. 2—Thermodynamic calculations of reference steel X2CrTiNb18 (*a*) Phase diagram (*b*) Volume fraction of phases (calculated with TCFe6.2).

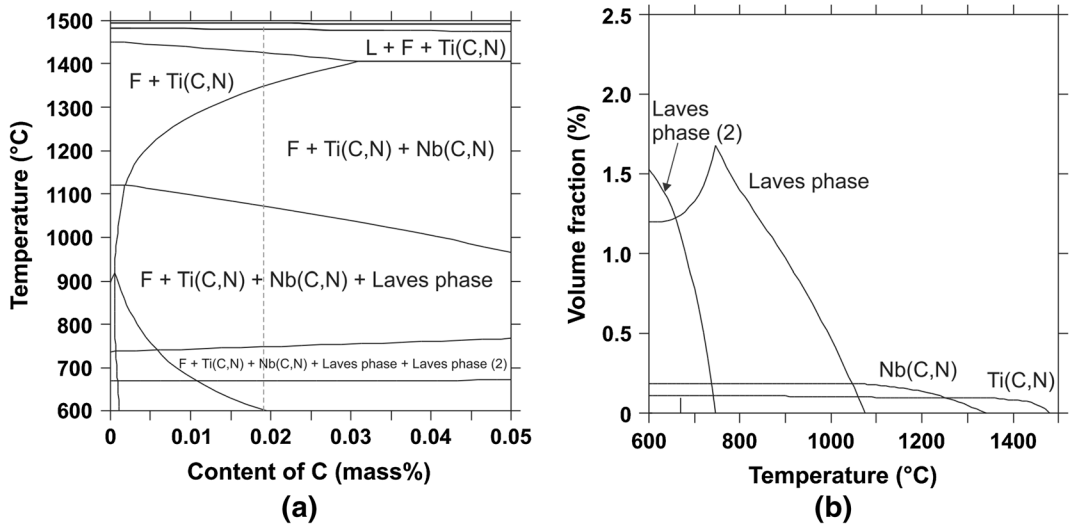

Fig. 3—Thermodynamic calculations of alloy Fe18CrW (*a*) Phase diagram (*b*) Volume fraction of phases (calculated with TCFe6.2).

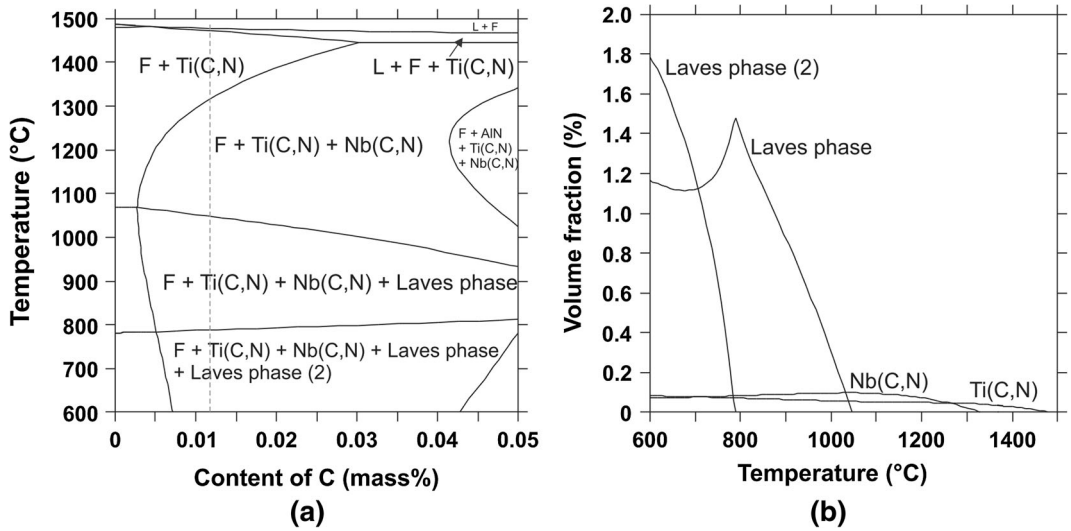

Fig. 4—Thermodynamic calculations of alloy Fe19CrWAl (*a*) Phase diagram (*b*) Volume fraction of phases (calculated with TCFe6.2).

Table II. Summary of the Calculated Phases and Temperatures for the Investigated Alloys (TCFe6.2)

Alloy	Solvus Temperature Laves [K (°C)]	Present Phases at 1173.15 K (900 °C)	Volume Fraction of Laves Phase (pct)
Fel9CrWAI	[1319 (1046)]	ferrite, Ti(C, N), Nb(C, N), Laves phase	0.88
Fe18CrW	[1348 (1075)]	ferrite, Ti(C, N), Nb(C, N), Lavas phase	0.97
Fel8CrMoW	[1342 (1069)]	ferrite, Ti(C, N), Nb(C, N), Laves phase	0.93
XlCrWNbTiLa22	[1224 (951)]	ferrite, Ti(C, N), Nb(C, N), Laves phase	0.32
X2CrTiNb18	[1198 (925)]	ferrite, Ti(C, N), Nb(C, N), Laves phase	0.11

Table III. Offset Yield Strength at 1173.15 K (900 °C) with Annealing Time of the FeCr Alloys (MPa)

$t_{annealing}$ (h)	X2CrTiNbl8	Fel8CrW	Fel8CrMo
Solution-annealed	31.3 ± 0.0	48.1 ± 2.0	49.8 ± 0.7
1	28.6 ± 0.0	43.0 ± 0.3	42.3 ± 2.2
24	26.9 ± 0.0	37.9 ± 1.9	38.2 ± 1.6
192	26.5 ± 0.0	35.6 ± 1.5	40.9 ± 2.8
720	—	42.6 ± 2.0	43.4 ± 1.1
1440	—	38.0 ± 0.5	38.1 ± 0.3

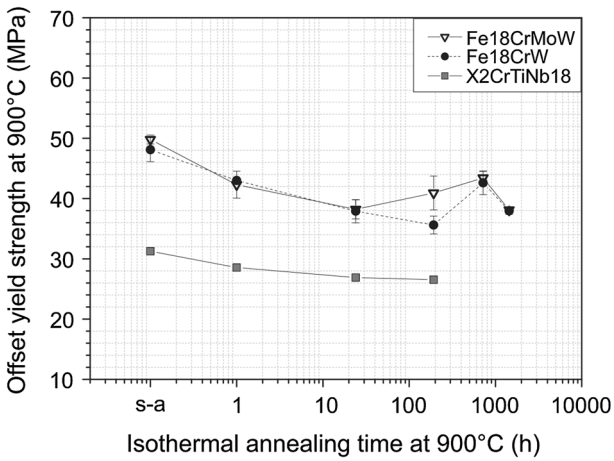

Fig. 5—Offset yield strength at 1173.15 K (900 °C) of the FeCr alloys in dependence of the isothermal annealing time.

F. *Measurement and Simulation of the Diffusion Profile in the Laves Phase Precipitate*

To confirm that the Laves phase is in a chemical equilibrium state, *ex situ* EDS was performed with linescans crossing a single Laves phase particle in steel Fe18CrMoW after 1440 hours annealing time (Figure 1). A gradient in the chemical composition, particularly of W and Nb, would have been detected if a chemical equilibrium had not been reached.

To eliminate the influence of the greater emissive volume of EDS measurements due to the different mean atomic numbers of the Laves phase (32.8 u) and in the matrix (25.9 u), Monte Carlo simulations of the measured EDS intensity were performed with WinCasino 2.48. The results of these simulations were then compared to the measured element profiles.

With this method, the inevitable blurring of a change in the composition due to the emissive volume could be

compared to the measured transition. These simulations can also be used to determine the minimum diameter of a W-depleted core that can be detected by EDS.

III. RESULTS AND DISCUSSION

A. *Alloy Design*

The alloy design concept focuses on increasing the high-temperature strength and long-term microstructural stability of ferritic heat-resistant steels at application temperatures of 1173.15 K (900 °C) and more. A combination of solid-solution and precipitation strengthening by Laves phase formation was thus used. Furthermore, the formation of a Laves phase should reduce the mobility of the grain boundaries to avoid grain growth during high-temperature service.

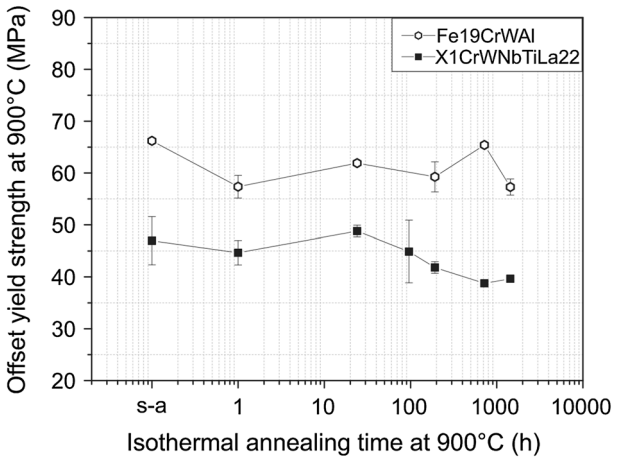

Fig. 6—Offset yield strength at 1173.15 K (900 °C) of the FeCrAl alloy compared to X1CrWNbTiLa22 in dependence of the isothermal annealing time.

Table IV. Offset Yield Strength at 1173.15 K (900 °C) with Annealing Time of the FeCrAl Alloys (MPa)

$t_{annealing}$ (h)	Fel9CrWAl	XlCrWNbTiLa22
Solution-annealed	66.2 ± 0.0	47.0 ± 4.6
1	57.4 ± 2.2	44.6 ± 2.3
24	61.9 ± 0.0	48.8 ± 1.1
192	59.3 ± 2.9	41.8 ± 1.1
720	65.4 ± 0.0	38.8 ± 0.6
1440	57.3 ± 1.6	39.6 ± 0.0

This alloy concept is based on the commercially available ferritic steels X1CrWNbTiLa22-2 and X2CrTiNb18. Steel X1CrWNbTiLa22-2 is mainly used for metallic interconnectors in planar SOFC. It contains 22 mass pct Cr, to provide a sufficient oxidation resistance, W, Nb, and Si, and it forms a Laves phase.[17] Steel X2CrTiNb18 also has a high Cr content (18 mass pct) and forms a Laves phase due to the elements Nb and Si.[17] This steel does not contain the element W. Its application field is in automotive exhaust systems.[18]

As can be seen from the calculated phase diagram in Figure 2, the solvus temperature of the Laves phase in steel X2CrTiNb18 is 1198.15 K (925 °C) and that of alloy X1CrWNbTiLa22-2 is 1224.15 K (951 °C). With demands for higher application temperatures up to 950 °C, the stability of the Laves phase in these alloys is insufficient. Therefore, the alloy design aimed to increase the solvus temperature of the Laves phase up to 1323.15 K (1050 °C). From the literature[19] and our previous investigations, Nb is known to be the most potent Laves phase former and its strong effect can be enhanced by combining it with Si.[20] However, low concentrations of C and N, which are unavoidable during steel production, decrease the solvus temperature of the Laves phase due to the high affinity of Nb for C and N, thus leading to the formation of carbides/nitrides instead of the Laves phase.[21] Microalloying with Ti minimizes primary precipitation of niobium nitrides and niobium carbides, so that this element is still available for Laves phase formation.

Three model alloys, namely Fe18CrW, Fe18CrMoW, and Fe19CrWAl were designed according to this alloy concept (Table I). Steel Fe19CrWAl was additionally alloyed with 3.5 mass pct Al and low

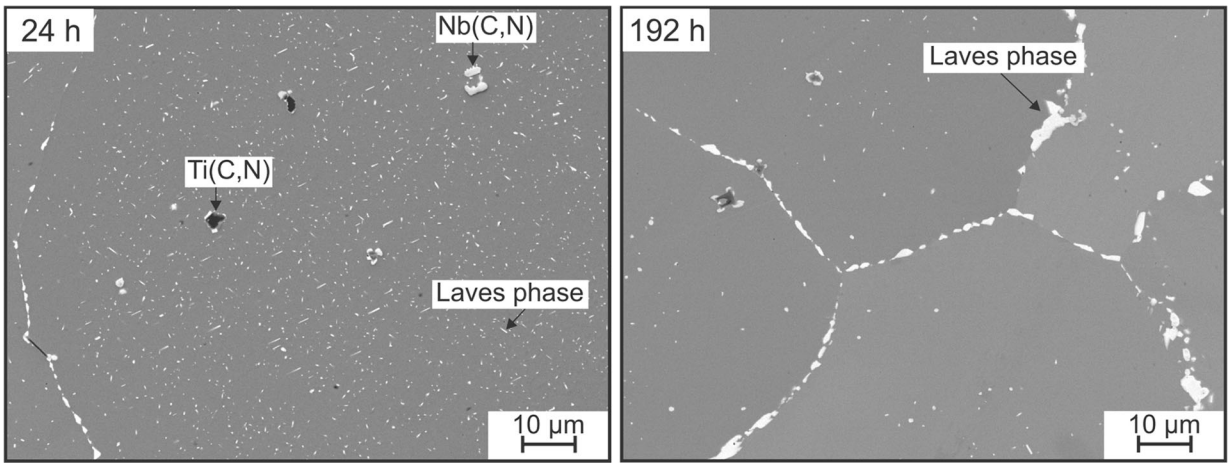

Fig. 7—Microstructure of steel Fe18CrW after 24 and 192 h annealing time at 1173.15 K (900 °C).

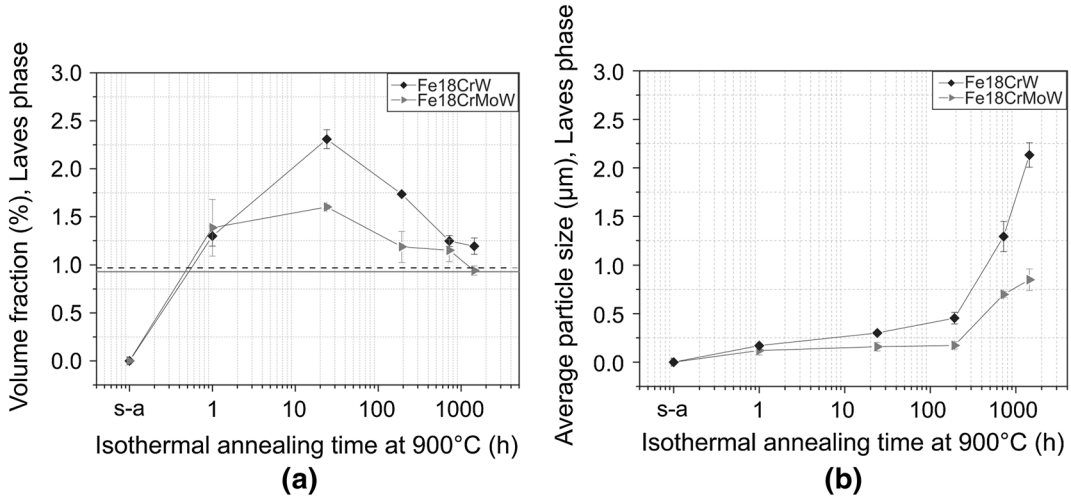

Fig. 8—Microstructure of alloys Fe18CrW and Fe18CrMoW in dependence of the annealing time at 1173.15 K (900 °C) (a) volume fraction of the Laves phase, (*b*) Average particle size of the Laves phase.

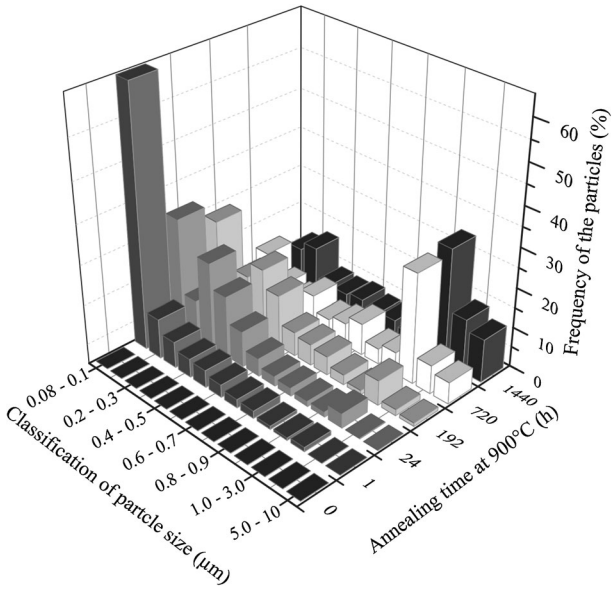

Fig. 9—Frequency of the Laves phase particles in alloy Fe18CrW in dependence of the annealing time at 1173.15 K (900 °C).

concentrations of the elements Hf, Zr, and Y in order to improve its oxidation resistance, which is required for applications in heat exchangers. The calculated phase diagrams and volume fractions of phases for alloys Fe18CrMoW and Fe19CrWAl are illustrated in Figures 3 and 4.

The calculated phase diagrams of alloys Fe18CrMoW and Fe19CrWAl show that the phase field around 1173.15 K (900 °C) contains ferrite, Ti-rich carbonitrides (Ti(C,N)), Nb-rich carbonitrides (Nb(C,N)), and a Laves phase of type Fe_2Nb as equilibrium phases. The calculated solvus temperatures of the Laves phase for the newly designed alloys and the reference steels are summarized in Table II. The solvus temperature of the Laves phase in the new steels is about 373.15 K (100 °C) higher than that of the reference steels.

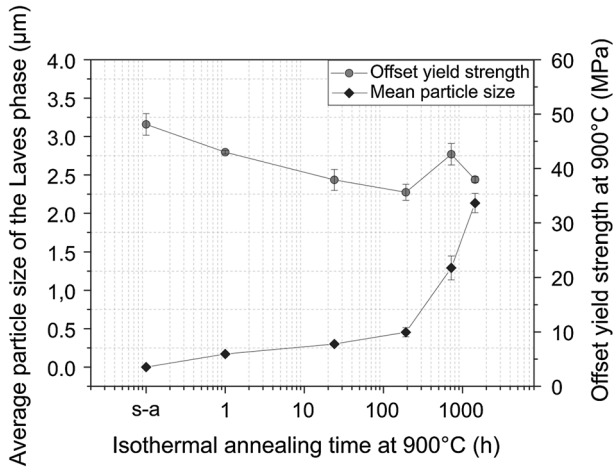

Fig. 10—Relationship between high-temperature strength and Laves phase particle size of steel Fe18CrW with annealing time.

B. *Influence of Long-term Annealing on High-Temperature Strength*

The alloying concept of ferritic materials Fe18CrW, Fe18CrMoW, and Fe19CrWAl is similar to that described above. However, steel Fe19CrWAl is alloyed with 3.5 mass pct aluminum and microalloyed with the elements Hf, Zr, and Y. This means that steel Fe19CrWAl differs from alloys Fe18CrW and Fe18CrMoW with respect to the oxide layer formed on its surface. Therefore, the newly designed alloys are considered separately and compared to the corresponding reference material.

The offset yield strength of alloys Fe18CrW, Fe18CrMoW, and X2CrTiNb18 at 1173.15 K (900 °C) (Table III) is plotted versus the isothermal annealing time in Figure 5. In the solution-annealed state (s-a), the offset yield strength of alloys Fe18CrW and Fe18CrMoW is about 18 MPa higher than that of reference steel X2CrTiNb18. On increasing the annealing time to 192 hours, the high-temperature strength of all alloys decreases (Figure 5). Even after long-term annealing, the

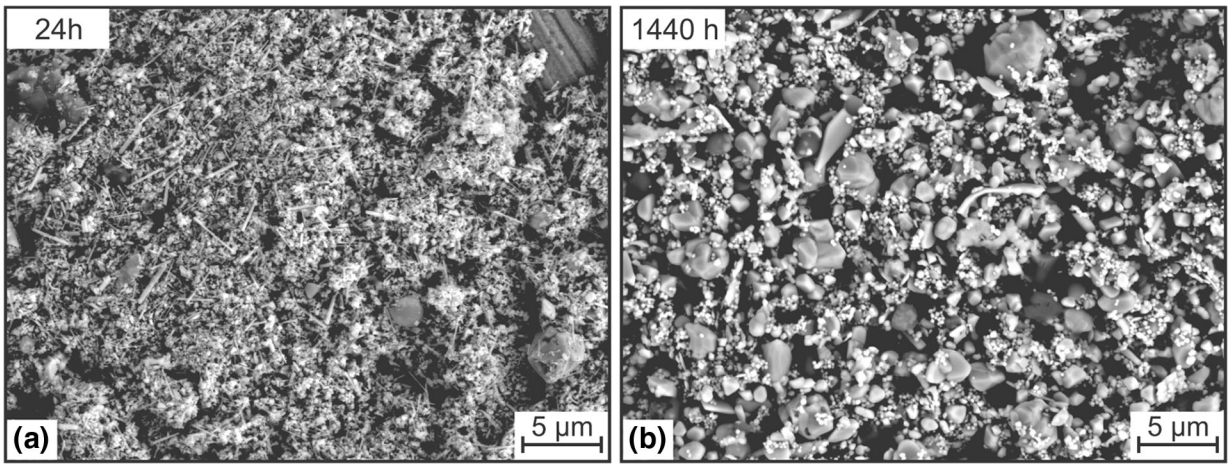

Fig. 11—Precipitate residue of alloy Fe18CrMoW after 24 and 1440 h annealing time.

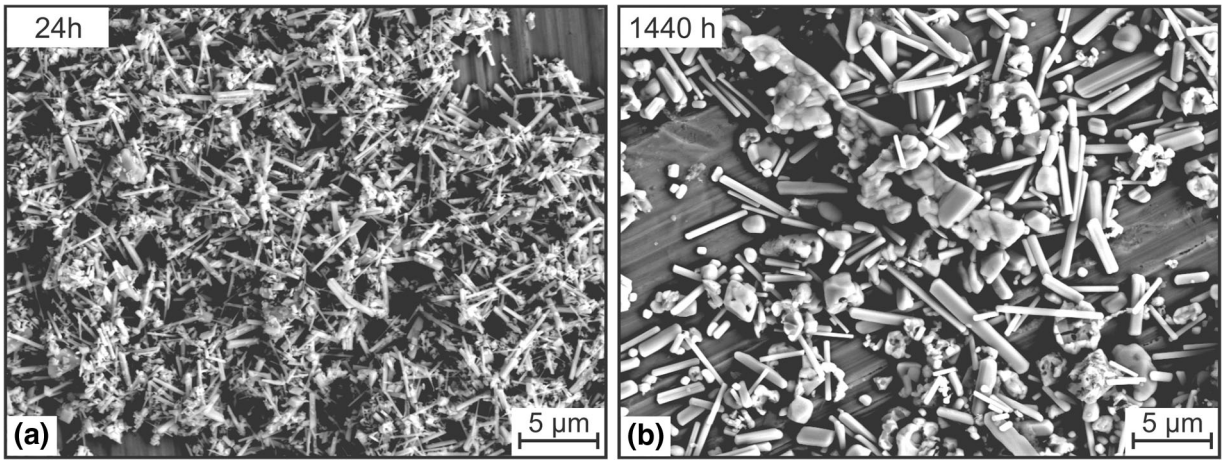

Fig. 12—Precipitate residue of alloy Fe19CrWAl after 24 and 1440 h annealing time.

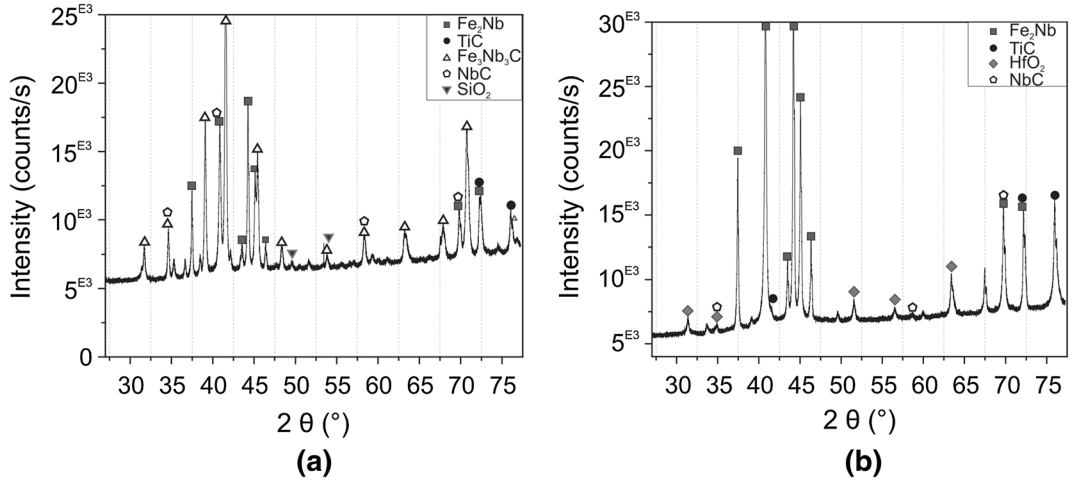

Fig. 13—Results of the XRD analyses (CuK_α, $\lambda = 1.54178$ Å) of the precipitate residue in alloys (*a*) Fe18CrMoW and (*b*) Fe19CrWAl.

offset yield strength of alloys Fe18CrW and Fe18CrMoW is higher than that of reference steel X2CrTiNb18.

The high-temperature strength of alloys Fe18CrW and Fe18CrMoW increases slightly after 720 hours annealing time. However, after 1440 hours dwell time at 1173.15 K (900 °C), the high-temperature strength of both alloys decreases again. Overall the high-temperature strength of the alloys Fe18CrW and Fe18CrMoW

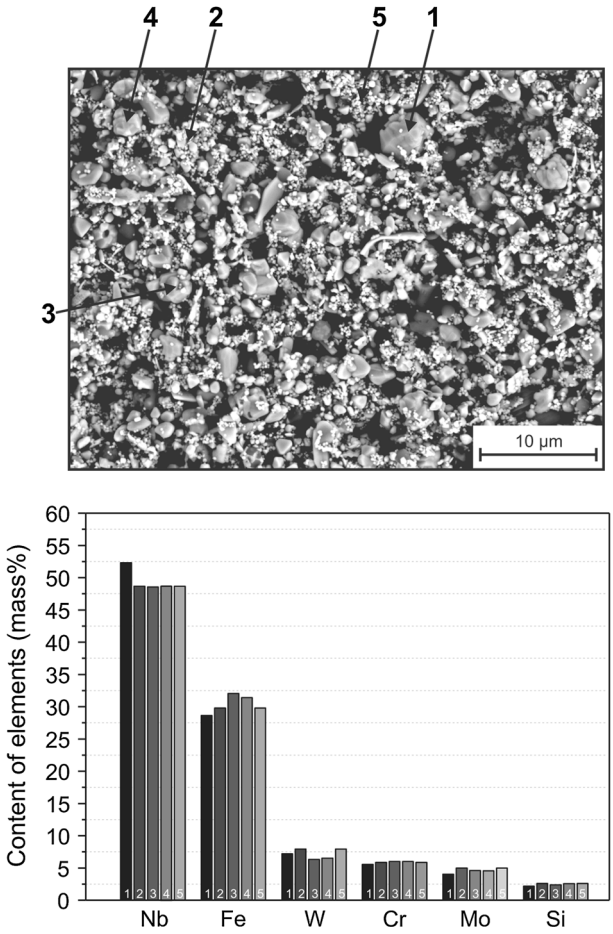

Fig. 14—EDS point measurements of the Laves phase particles in alloy Fe18CrMoW after annealing at 1173.15 K (900 °C) for 1440 h.

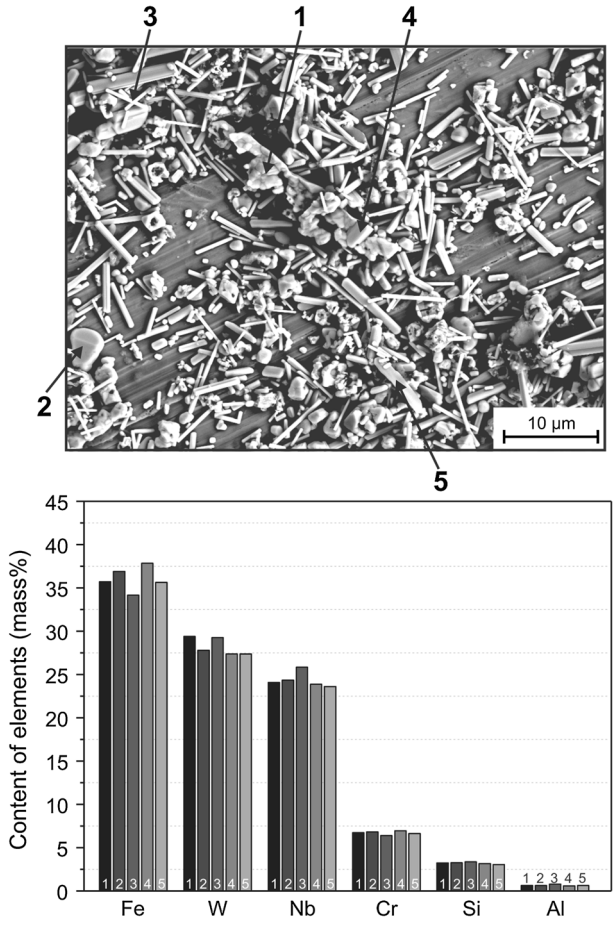

Fig. 15—EDS point measurements of the Laves phase particles in alloy Fe19CrWAl after annealing at 1173.15 K (900 °C) for 1440 h.

decreases by about 10 MPa with respect to the annealing time (1440 hours) (Figure 5).

The difference in the high-temperature strength between the newly designed alloys and the reference steel is attributed to the solid-solution strengthening effect of the elements W and/or Mo.[1,19,22,23] According to Fujita *et al.*,[1] an addition of 2 mass pct W or 1,5 mass pct Mo in ferritic stainless steels leads to an enhancement of the high-temperature strength by solid-solution strengthening. In the case of the Al-alloyed steel Fe19CrWAl the offset yield strength at 1173.15 K (900 °C) is about 66 MPa in the solution-annealed state (s-a), as can be seen in Figure 6 and Table IV. After 1 hours annealing time at 1173.15 K (900 °C) the offset yield strength decreases by about 9 MPa. On further annealing, the high-temperature strength decreases non-monotonically (Figure 6). Overall, steel Fe19CrWAl exhibits a reduction of 9 MPa after long-term annealing for 1440 hours. The Al-free reference steel X1CrWNb-TiLa22-2 shows a continuous decrease with annealing time. After 1440 hours annealing time, the reduction of the high-temperature strength is about 7 MPa (Figure 6).

In order to understand the reduction of high-temperature strength in dependence of the annealing time, the microstructure of all three newly designed alloys was investigated in different annealing states. In the solution-annealed state, alloy Fe18CrW has a mean grain size of 114 μm, which increases to 126 μm after long-term annealing. Hence, only minimal grain growth takes place during annealing at 1173.15 K (900 °C). Alloys Fe18CrMoW and X2CrTiNb18 show similar behavior. Consequently, the reduction in high-temperature strength during annealing cannot be explained by pronounced grain growth. Thus, formation and coarsening of the Laves phase is a possible explanation for the reduction in high-temperature strength on increasing the annealing time.

C. *Effect of Laves Phase Formation and Subsequent Coarsening on the High-Temperature Strength*

The effect of the Laves phase on the high-temperature strength and creep resistance in ferritic stainless steels is a controversial topic in the literature. Fujita *et al.*[1] report that, in addition to the solid-solution strengthening in ferritic Nb-added stainless steels, dynamic precipitation strengthening by the precipitates of carbides, nitrides, and the Laves phase formed during tensile testing also contribute to the improvement the high-temperature strength. However, longer annealing times at high temperatures [973.15 K to 1173.15 K

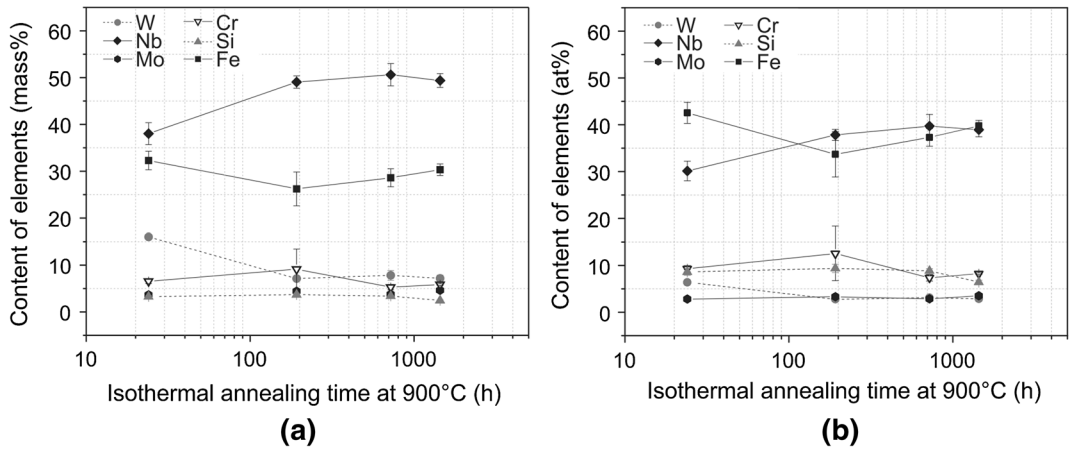

Fig. 16—Evolution of the Laves phase in steel Fe18CrMoW during annealing at 1173.15 K (900 °C).

Table V. Evolution of the Chemical Composition of the Laves Phase in Alloy Fe18CrMoW in Dependence of the Annealing Time at 1173.15 K (900 °C) (determined by EDS)

$t_{annealing}$ (h)	Fe mass pct	Nb mass pct	W mass pct	Cr mass pct	Si mass pct	Mo mass pct
24	32.3 ± 2.0	38.0 ± 2.3	16.0 ± 0.2	6.6 ± 0.5	3.3 ± 0.2	3.7 ± 0.3
192	26.2 ± 3.6	49.1 ± 1.3	7.1 ± 0.1	9.1 ± 4.3	3.7 ± 0,3	4.4 ± 0.5
720	28.6 ± 1.9	50.6 ± 2.4	7,8 ± 1.0	5.3 ± 0.6	3.4 ± 9,1	3.8 ± 0.4
1440	30.3 ± 1.2	49.4 ± 1.5	7.2 ± 0.7	5.9 ± 0.2	2.5 ± 0.2	4.6 ± 0.4
	at. pct	at. pct	at. pct	at. pct	at. pct	at. pct
24	42.5 ± 2.3	30.1 ± 2.1	6.4 ± 0.0	9.3 ± 0.7	8.6 ± 0.7	2.8 ± 0.2
192	33.7 ± 4.8	37.8 ± 1.2	2.8 ± 0.1	12.6 ± 5.8	9.4 ± 0.9	3.3 ± 0.4
720	37.3 ± 1.9	39.7 ± 2.5	3.1 ± 0.5	7.4 ± 0.7	8.9 ± 0.4	2.9 ± 0.3
1440	39.8 ± 1.2	38.9 ± 1.5	2.9 ± 0.3	8.3 ± 0.2	6.4 ± 0.4	3.5 ± 0.3

(700 °C to 900 °C)] of Nb-added ferritic stainless steels lead to a reduction in the high-temperature strength due to microstructural changes during the annealing dwell time.[1,11,12,24,25] Froitzheim *et al.*,[17] Chiu and Lin[25] and Kuhn *et al.*[24] attribute the significantly improved creep resistance of steel X1CrWNbTiLa22-2 to the precipitation of Laves phase, whereby the extent of the improvement depends on the volume fraction and particle size of the Laves phase, which changes during long-term annealing.

To evaluate the contribution of Laves phase formation and coarsening in the newly designed alloys, the volume fraction and particle size of the Laves phase were determined in dependence of the annealing time. Figure 7 shows the microstructure of alloy Fe18CrW after 24 and 192 hours isothermal annealing at 1173.15 K (900 °C). Two types of carbonitrides (Nb(C,N), Ti(C,N)), and a Laves phase (Fe_2Nb) were observed in the microstructure. Figures 8a, b shows the experimentally determined volume fraction and average particle size of the Laves phase in alloys Fe18CrW and Fe18CrMoW in dependence of the annealing time at 1173.15 K (900 °C). In the solution-annealed state, no Laves phase was found in either of the steels. After 1 hour annealing time, more than 1 vol pct Laves phase had formed. On increasing the annealing time up to 24 hours, the Laves phase volume fraction in steel Fe18CrW increased up to 2 vol pct, whereas alloy Fe18CrMoW showed a smaller increase. With longer annealing times, both alloys show a decrease in the Laves phase volume fraction. Alloys Fe18CrW and Fe18CrMoW exhibit a Laves phase volume fraction of 1.1 and 0.95 vol pct, respectively, after 1440 hours isothermal annealing time at 1173.15 K (900 °C). The calculated values are 0.97 vol pct for steel Fe18CrW and 0.93 vol pct for steel Fe18CrMoW (marked in Figure 8a), which agree well with the measured results. Consequently, the volume fraction of the Laves phase in both alloys converges to the calculated equilibrium state after 1440 hours annealing time.

The mean particle size of alloys Fe18CrW and Fe18CrMoW is about 0.2 μm after 1 hour annealing (Figure 8b). With longer annealing times the mean particle size of the Laves phase of both steels increases significantly. After 1440 hours annealing, alloys Fe18CrW and Fe18CrMoW exhibit an increase in the particle size by about 1.9 and 0.6 μm, respectively (Figure 8b). Simultaneously, the microstructure undergoes Ostwald ripening during annealing at 1173.15 K (900 °C), in which the fine precipitates dissolve in favor of the coarse particles.[26] Figure 9 shows the classification of the Laves phase particle size in dependence of the annealing time for alloy Fe18CrW. The fraction of fine particles (0.08 to 0.1 μm) is about 60 pct after 1 hour. With longer annealing times, the fraction of fine particles decreases, whereas the fraction of coarse particles (1 to 3 μm) increases by 30 pct. This realign-

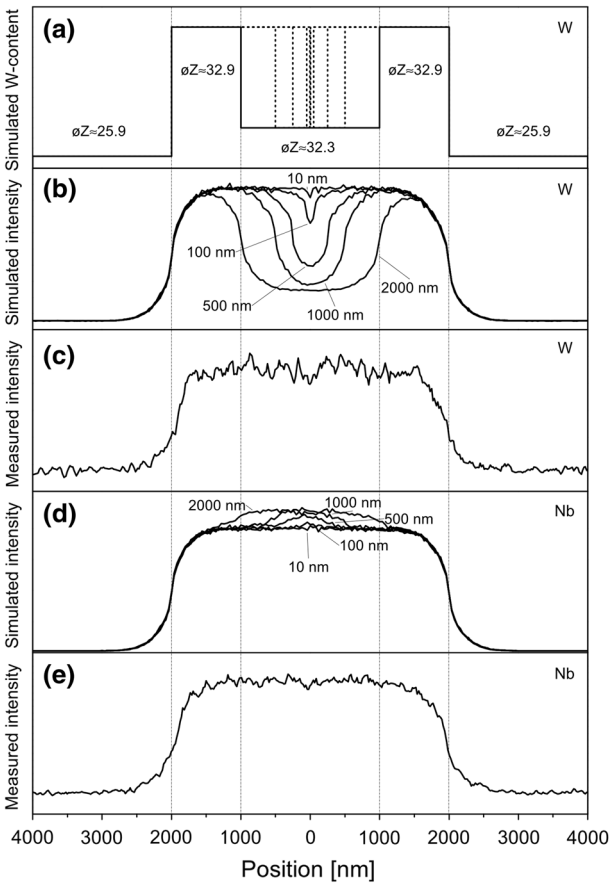

Fig. 17—Measured and simulated intensity of W and Nb in a line-scan over a Laves phase precipitate in steel Fe18CrMoW after annealing for 1440 h at 1173.15 K (900 °C). The simulated precipitate contained a W-depleted core with a diameter ranging from 102000 (*a*), the corresponding simulation result is marked with an arrow and the core diameter (W in *b* and Nb in *d*). The measured EDS profiles for Nb and W are shown in c and e. The measured precipitate is shown in Figure 1. An acceleration voltage of 20 was used in the simulation and for the measurements. The simulation was performed with WinCasino 2.48.

ment of the Laves phase can be seen in the microstructure of different annealing states in Figure 7.

Hence, rapid coarsening of the Laves phase takes place in both investigated steels. These findings agree with the results of Sim *et al.*,[12] who investigated the coarsening behavior of the Laves phase in ferritic stainless steels at 1173.15 K (900 °C). They explain the rapid coarsening rate of the Laves phase by the incoherent interface between the ferritic matrix and the Laves phase precipitates.[12]

Owing to rapid coarsening of the Laves phase, their contribution to the high-temperature strength via precipitation hardening is debatable. Figure 10 shows the offset yield strength at 1173.15 K (900 °C) and the average particle size of the Laves phase in steel Fe18CrW in dependence of the annealing time. In the solution-annealed state the high-temperature strength is about 48 MPa. After 1 hour annealing time, the offset yield strength decreases, whereas the Laves phase particles coarsen by about 0.2 μm. With longer annealing times, the average particle size of the Laves phase increases and simultaneously the high-temperature strength decreases slightly. Therefore, it can be stated that the contribution of the Laves phase to the high-temperature strength is comparatively low due to the rapid coarsening. Additionally, the increase of the yield strength after annealing for 720 hours can not be a result of the higher particle size.

Li[10] reports that the size of the Laves phase plays a very important role with respect to strengthening. Larger particle sizes decrease the dislocation pinning efficiency of the Laves phase precipitates.[10]

Fujita, Miyazaki, and Sim *et al.*[11,12,27] argue that precipitation of the Laves phase (Fe_2Nb) in ferritic stainless steel is detrimental to the high-temperature strength. They report that during isothermal annealing at high temperatures [973.15 K to 1173.15 K (700 °C to 900 °C)], the Nb content in the matrix decreases due to the precipitation of a Nb-rich Laves phase (Fe_2Nb). This decrease in the Nb content in the ferritic matrix leads to loss of the solid-solution strengthening effect of Nb and the high-temperature strength decreases.[11,12,27] Further analyses were carried out to confirm this theory.

D. *Evolution of Chemical Composition of the Laves Phase During Long-term Annealing*

Evolution of Nb phases during annealing was investigated by determining, the chemical composition of the Laves phase in steels Fe18CrMoW and Fe19CrWAl in different annealing states. For accurate chemical measurements, the precipitates were isolated from the matrix and the residue powders were analyzed.

Figures 11 and 12 show the microstructure of the precipitate residue of alloys Fe18CrMoW and Fe19CrWAl after 24 and 1440 hours annealing time. After 24 hours annealing time, steel Fe18CrMoW contains fine acicular particles (<1 μm) as well as spherical coarse particles of about 3 μm (Figure 11a). Longer annealing times lead to a change in the particle shape and also significant coarsening takes place (Figure 11b). In contrast to this, the precipitate residue of alloy Fe19CrWAl exhibits an acicular shape after 24 hours annealing time, which remains unchanged with longer annealing times (Figures 12a, b).

The phases present in the residue powders of alloys Fe18CrMoW and Fe19CrWAl were identified by means of XRD analyses. Figure 13a shows the results of the XRD analyses of the residue of steel Fe18CrMoW after 24 hours annealing time. Laves phase of type Fe_2Nb, as well as Ti-rich and Nb-rich carbides, Si-rich oxides, and carbides of type Fe_3Nb_3C were observed. In the case of alloy Fe19CrWAl, Laves phase of type Fe_2Nb, Ti-rich and Nb-rich carbides, and Hf-rich oxides were detected (Figure 13b). Alloy Fe19CrWAl does not form carbides of type Fe_3Nb_3C in contrast to steel Fe18CrMoW. The formation of Fe_3Nb_3C depends on the C content in the matrix. Steel Fe19CrWAl is microalloyed with the elements Hf and Zr, which have a high affinity for C and N, so that formation of Fe_3Nb_3C is avoided.

This means that the residue powder contains several phases. As can be seen in Figure 11, the morphology of each particle varies in size and shape. In order to find

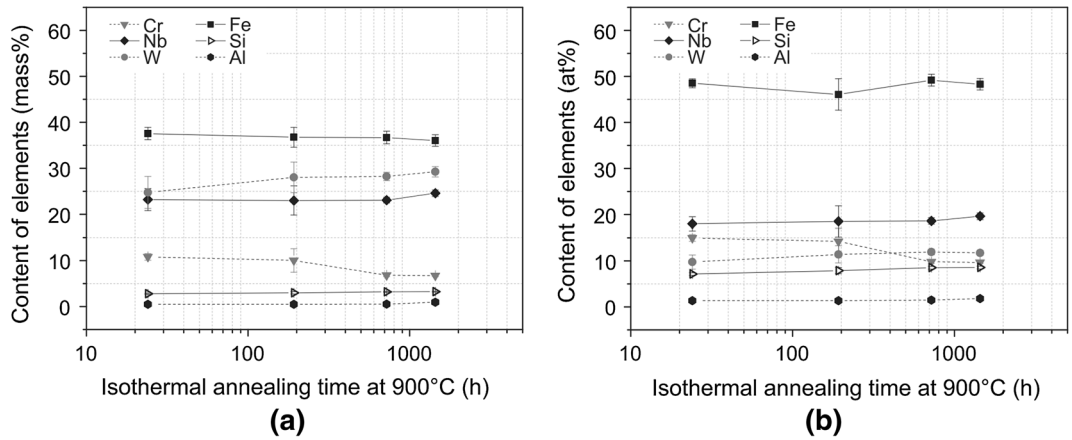

Fig. 18—Evolution of the Laves phase in steel Fe19CrWAl during annealing at 1173.15 K (900 °C).

Table VI. Evolution of the Chemical Composition the Laves Phase in Alloy Fe19CrWAl in Dependence of the Annealing Time at 1173.15 K (900 °C) (determined by EDS)

$t_{annealing}$ (h)	Fe mass pct	Nb mass pct	W mass pct	Cr mass pct	Si mass pct	Al mass pct
24	37.6 ± 1.3	23.2 ± 2.4	24.8 ± 3.5	10.8 ± 0.7	2.8 ± 0.1	0.5 ± 0.1
192	36.8 ± 2.1	23.0 ± 3.2	28.0 ± 3.3	10.0 ± 2.6	3.0 ± 0.2	0.5 ± 0.1
720	36.7 ± 1.4	23.1 ± 0.6	28.2 ± 0.9	6.8 ± 0.3	3.2 ± 0.1	0.5 ± 0.0
1440	36.0 ± 1.3	24.6 ± 0.7	29.3 ± 1.1	6.7 ± 0.2	3.2 ± 0.1	0.9 ± 0.6
	at. pct	at. pct	at. pct	at. pct	at. pct	at. pct
24	48.5 ± 1.0	18.0 ± 1.5	9.8 ± 1.5	15.0 ± 0.7	7.1 ± 0.3	1.3 ± 0.2
192	46.1 ± 3.4	18.5 ± 3.4	11.4 ± 1.9	14.2 ± 2.9	7.9 ± 0.7	1.4 ± 0.2
720	49.2 ± 1.3	18.6 ± 0.7	11.9 ± 0.6	9.8 ± 0.3	8.5 ± 0.3	1.5 ± 0.1
1440	48.3 ± 1.3	19.6 ± 0.7	11.7 ± 0.6	9.7 ± 0.2	8.6 ± 0.3	1.8 ± 0.2

Table VII. Comparison Between EDS and ICP-OES Measurements of the Chemical Composition of the Laves Phase in Alloy Fe19CrWAl after 192 h Annealing Time

	Fe	Nb	W	Cr	Si	Al
ICP-OES	33.00	27.0	21.0	6.2	2.7	0.4
EDS	36.8 ± 2.1	23.0 ± 3.2	28.0 ± 3.3	10.0 ± 2.6	3.0 ± 0.2	0.5 ± 0.1

differences in the chemical composition of the particles in dependence of the shape, five EDS point measurements of various particles were carried out. The resulting chemical composition after annealing at 1173.15 K (900 °C) for 1440 hours are shown in Figures 14 and 15. In the case of steel Fe18CrMoW, the Nb content was about 48 mass pct, in all measurements except for the first one (Figure 14). This affected the Fe content as seen in measurement 1 with the lowest Fe value. Overall, there is no significant difference in chemical composition of the various Laves phase particles in alloy Fe18CrMoW. In the case of alloy Fe19CrWAl, the measurements show slight differences in the Fe, W, and Nb contents, although, no significant differences are observed in particles of different size (Figure 15).

Owing to the small size of the Laves phase particles, the emissive volume of the EDS measurement may exceed the volume of one particle, and thus the measured chemical composition could be influenced by the surrounding particles. According to Monte Carlo simulations, the emissive volume of the EDS measurement in the Laves phase affects a region about 320 nm in width and 550 nm in depth, at most. Hence, the surrounding particles have an insignificant effect on the measured values.

Evolution of the chemical composition of the Laves phase during annealing was determined by EDS measurements on the precipitate residues of alloys Fe18CrMoW and Fe19CrWAl in different annealing states. The content of the elements is plotted against the annealing time for steel Fe18CrMoW in Figure 16. The measured values are summarised in Table V. After 24 hours annealing time, the average Nb content is 38 mass pct (30 at. pct) and the Fe content is 32 mass pct (42,5 at. pct) (Figure 16. After 192 hours annealing time, the Nb content increases by about 11 mass pct and the Fe content decreases by about 6 mass pct. With longer annealing times, there is no significant change in the Nb content, whereas the Fe content increases slightly (Figure 16). The W content decreases from 16 to 6 mass pct after 24 hours annealing time, but remains constant for longer annealing times. This means that

after 192 hours annealing time the Laves phase reaches a state close to the chemical equilibrium.

To confirm that the Laves phase is in a chemical equilibrium state, ex situ EDS was performed with linescans crossing a single Laves phase particle in steel Fe18CrMoW after 1440 hours annealing time (Figure 1). The results of one EDS linescan are shown in Figure 17. There is a smooth transition in W- and Nb intensity from the matrix to the precipitate, which seems to indicate a gradient in the chemical composition as a result of diffusion. Inside the precipitate, there are no significant intensity peaks that would indicate a W-depleted and Nb-enriched core.

In order to exclude a narrow gradient resulting from the bigger emissive volume during EDS measurement, Monte Carlo simulations were carried out with a particle of the same diameter and composition as that measured in a surrounding matrix. Additionally, a W-depleted and Nb-enriched core was created with a diameter ranging from 10 to 2000 nm. According to the simulation, the minimum detectable core diameter is 500 nm using the Nb signal and 100 nm using the W signal.

A comparison of the measured intensity of W with the simulated intensity on the interface between the matrix and the precipitate (Figures 17b, c) did not reveal a significant difference among both profiles. Since the underlying chemical composition of the phases is constant in the simulation (Figure 17a), this leads to the conclusion that the real chemical composition, used as a basis for the measured intensity, is also constant. The same logic applies to the measured and simulated intensity of Nb (Figures 17d, e).

The results thus confirmed that the Laves phase precipitates in steel Fe18CrMoW are in a state of chemical equilibrium after an annealing time of 1440 hours at 1173.15 K (900 °C). Furthermore, the presence of a core within the precipitate with a lower W content and a higher Nb content, and a diameter larger than 10 nm was ruled out.

The chemical composition of the Laves phase in steel Fe19CrWAl mainly consists of Fe, W, and Nb, whereby the W content is significantly higher than in alloy Fe18CrMoW (Figure 18). After 24 hours, the Fe content is 37.5 mass pct (48.5 at. pct), the W content 25 mass pct (10 at. pct), and the Nb content 23 mass pct (18 at. pct) (Figure 18; Table VI). With longer annealing times, the Fe content decreases slightly and the W content increases by about 3 mass pct. Overall, there is no significant change in the chemical composition of the Laves phase in alloy Fe19CrWAl during long-term annealing.

The residue of steel Fe19CrWAl was also analyzed by ICP-OES to corroborate the EDS measurements. Table VII lists the results together with those of the EDS measurements. These results confirm that the Laves phase mainly consists of the elements Fe, Nb, W, and Cr. The Fe content found by the EDS and ICP-OES measurements differ by about 8 pct, but this is within the usual range of error. The Nb content differs by about 4 mass pct owing to the fact that the ICP-OES chemical analyses measures all phases present in the extracted residue. This means that the Nb-rich carbides in the residue affect the results. The most significant difference is in the W content with 7 mass pct (Table VII).

The Laves phase formed in steel Fe18CrMoW differs in morphology and chemical composition from that in steel Fe19CrWAl. The shape of a precipitate is generally a compromise between a minimum distortion energy and the total surface energy.[28] On the other hand, the distortion energy depends on the interface energy between the precipitate and matrix.[28] For this reason, further investigations of the interface energy between the Laves phase precipitates and the matrix in both steels should be performed in order to understand differences in Laves phase formation. Of particular importance is the influence of the dissolved Al in steel Fe19CrWAl on the interface energy and also diffusion of the elements within the Laves phase.

Overall, it can be stated that the Laves phase in steel Fe18CrMoW achieves its chemical equilibrium after 192 hours annealing time, after which no significant change in the Nb content was measured. Nevertheless, the high-temperature strength decreases slightly. In the case of alloy Fe19CrWAl, the high-temperature strength also decreases slightly, although the Nb content does not change after only 24 hours annealing time. Consequently, the reduction in the high-temperature strength cannot be caused only by the change in Nb content with the annealing time. Instead, it is a combined effect of all microstructural changes, namely formation and coarsening of the Laves phase, evolution of its volume fraction and dispersion as well as depletion of alloying elements from the ferritic matrix.

IV. CONCLUSIONS

The present study has focused on the effect of Laves phase precipitates on the high-temperature strength of three newly designed ferritic stainless steels during isothermal long-term annealing. Based on the present results, the following conclusions can be drawn:

1. Due to the solid-solution strengthening effect of W as well as Mo, the high-temperature strength of ferritic stainless steel was increased and this enhancement was preserved during long-term annealing.
2. The addition of 3.5 mass pct Al leads to an increase in the high-temperature strength of the ferritic stainless steels due to a solid-solution strengthening effect.
3. Investigations of the microstructure in dependence of the annealing time at 1173.15 K (900 °C) showed rapid growth and coarsening of Laves phase precipitates.
4. Due to the rapid coarsening of the Laves phase precipitates, their contribution to the high-temperature strength via precipitation hardening is comparatively small. However, their coarsening is also not detrimental to the high-temperature strength. Formation of the Laves phase along grain boundaries avoids grain growth during long-term annealing.

5. The Laves phase residue extracted from Al-alloyed steels differs in morphology and chemical composition compared to Al-free steels.
6. The chemical composition of the Laves-phase in Al-free ferritic steels achieves its equilibrium state after 192 hours annealing time, whereas this condition is reached in the Al-alloyed steels after 24 hours annealing time.

ACKNOWLEDGMENTS

The authors gratefully acknowledge financial support by the Bundesministerium für Bildung und Forschung (BMBF) for the project ''Entwicklung von Höchstleistungswerkstoffen für Hochtemperatur-Wärmetauscher und PKW-Abgasanlagen'' (''Development of high-performance materials for high-temperature heat carriers and automotive exhaust systems'') under Contract number 03X3520G.

REFERENCES

1. N. Fujita, K. Ohmura, M. Kikuchi, T. Suzuki, S. Funaki, and I. Hiroshige: *Scripta Mater*., 1996, vol. 35 (6), pp. 705–10.
2. W. Quadakkers, J. Piron-Abellan, V. Shemet, and L. Singheiser: *Mater. High Temp*., 2003, vol. 20 (2), pp. 115–27.
3. T.J. Nichol, A. Datta, and G. Aggen: *Metall. Trans. A*, 1980, vol. 11 (4), pp. 573–85.
4. A. van Zwieten and J. Bulloch: *Int. J. Press. Vessels Pip*., 1993, vol. 56 (1), pp. 1–31.
5. H. Berns and W. Theisen: *Ferrous materials: Steel and cast iron*, Springer, Berlin, 2008.
6. Y. Inoue and M. Kikuchi: *Nippon Steel Technical Report*, 2003, pp. 62–69.
7. F. Chassagne, J. Mithieux, and J. Schmitt: *Steel Res. Int*., 2006, vol. 77 (9–10), pp. 680–85.
8. P.O. Santacreu, O. Cleizergues, C. Simon, and P. Duroux: *Revue De Metallurgie-Cahiers D Informations Techniques*, 2004, vol. 101 (7–8), pp. 615–20.
9. F. Abe: *Metall. Mater. Trans. A*, 2005, vol. 36A, pp. 321–32.
10. Q. Li: *Metall. Mater. Trans. A*, 2006, vol. 37A, pp. 89–97.
11. A. Miyazaki, K. Takao, and O. Furukimi: *ISIJ Int*., 2002, vol. 42 (8), pp. 916–20.
12. G.M. Sim, J.C. Ahn, S.C. Hong, K.J. Lee, and K.S. Lee: *Mater. Sci. Eng., A*, 2005, vol. 396 (1–2), pp. 159–65.
13. H.L. Lukas, S.G. Fries, and B. Sundman: *Computational Thermodynamics: The CALPHAD Method*, Cambridge University Press, Cambridge, 2007.
14. Thermo-Calc Software: *Thermo-Calc—User's Guide—Version S*. Stockholm and Schweden, 2008.
15. T. Sawatani, S. Minamino, and H. Morikawa: *Trans. Iron Steel Inst. Jpn*., 1982, vol. 22 (3), pp. 172–80.
16. H. Kutsumi, A. Chino, and Y. Ishibashi: *Tetsu to Hagane-J. Iron Steel Inst. Jpn*., 1992, vol. 78 (4), pp. 594–600.
17. J. Froitzheim, G. Meier, L. Niewolak, P. Ennis, H. Hattendorf, L. Singheiser, and W. Quadakkers: *J. Power Sources*, 2008, vol. 178 (1), pp. 163–73.
18. M. Sello and W. Stumpf: *Mater. Sci. Eng., A*, 2010, vol. 527 (20), pp. 5194–202.
19. V. Knežević, J. Balun, G. Sauthoff, G. Inden, and A. Schneider: *Mater. Sci. Eng., A*, 2008, vol. 477 (1–2), pp. 334–43.
20. N. Nabiran, S. Weber, and W. Theisen: *Steel Res. Int*., 2012, vol. 83 (8), pp. 758–65.
21. W. Gordon and A. van Bennekom: *Mater. Sci. Technol*., 1996, vol. 12 (2) pp. 126–31.
22. D. Rojas, J. Garcia, O. Prat, C. Carrasco, G. Sauthoff, and A. Kaysser-Pyzalla: *Mater. Sci. Eng., A*, 2010, vol. 527 (16–17), pp. 3864–76.
23. Y. Kato, A. Miyazaki, and T. Ujiro: JFE Steel*JP*, 2008, vol. 20, pp. 28–32.
24. B. Kuhn, C.A. Jimenez, L. Niewolak, T. Hüttel, T. Beck, H. Hattendorf, L. Singheiser, and W. Quadakkers: *Mater. Sci. Eng., A*, 2011, vol. 528 (18), pp. 5888–99.
25. Y. Chiu and C. Lin: *J. Power Sources*, 2012, vol. 198, pp. 149–57.
26. P.W. Voorhees: *J. Stat. Phys*., 1985, vol. 38 (1–2), pp. 231–52.
27. N. Fujita, K. Ohmura, and A. Yamamoto: *Mater. Sci. Eng., A*, 2003, vol. 351 (1–2), pp. 272–81.
28. G. Gottstein: *Physical Foundations of Material Science*, Springer, Berlin, 2004.